Available online at www.sciencedirect.com
ScienceDirect
Journal of the European Ceramic Society 28 (2008) 965–971
www.elsevier.com/locate/jeurceramsoc

# Ceramic oxide electrolytes based on $CeO_2$—Preparation, properties and possibility of application to electrochemical devices

Magdalena Dudek *

*AGH-University of Science and Technology, Faculty of Materials Science and Ceramics, al. Mickiewicza 30/312, 30-059 Cracow, Poland*

Available online 17 October 2007

**Abstract**

Samples of pure $CeO_2$, $Ce_{1-x}Sm_xO_2$, $Ce_{1-x}(Sm_{0.5}Ca_{0.5})_xO_2$, where $0<x<0.25$ or $Ce_{0.2-x}Sm_xY_xO_2$, within $0<x<0.2$ were sintered from fine powders obtained by the citrate method. The preparation method, microstructure, and structure of samples are presented and discussed. All powders and sinters were found to be ceria-based solid solutions of the fluorite type structure. The results of hardness, fracture toughness measurements are reported. The results of electrical properties of the samples investigated by an ac impedance spectroscopy in temperature range 150–700 °C and for frequency range $10^{-2}$ to $10^7$ Hz are also presented and discussed. The electrical properties of ceria co-doped with $Sm_2O_3$ and $Y_2O_3$ or CaO and $Sm_2O_3$ samples are found to be improved very little compared to only the samaria or yttria-doped ceria. The best oxygen ion conductivity was found for the $Ce_{0.8}Sm_{0.1}Y_{0.1}O_2$ compound. Testing results of this compound used as an electrolyte in oxygen-concentration cell are also reported.


*Keywords:* Electrical properties; $CeO_2$; Fuel cells; Sensors; Ionic conductivity

## 1. Introduction

Until now ($Y_2O_3$ or CaO)–$ZrO_2$-based solid solutions are extensively used as solid electrolytes in solid oxide fuel cells, electrochemical gas sensors, oxygen pumps, probes for determination oxygen dissolved in liquid metal alloys. This is due to its low electronic and high oxygen ionic conductivity, chemical stability in oxidizing and reducing atmospheres at high temperatures and relatively low production cost.[1,2] Solid oxide fuel cells (SOFC) using stabilized $ZrO_2$ with 8% mol $Y_2O_3$ (8YSZ) as solid electrolyte requires high operating temperature 900–1000 °C, resulting in serious problems such as chemical reaction between components, thermal degradation of materials or cracking during cycles. This implies a short service life of the cell and requires expensive metallic materials for interconnectors. Lowering the operation temperature of a SOFC to 600–700 °C gives the opportunity for iron-based alloys (Fe–Cr) to be used as materials for interconnects of so-called intermediate temperature solid oxide fuel cell (IT-SOFC).[3,4]

Rare earth doped ceria $Ce_{1-x}Me_xO_2$ (Me = Sm, Gd) and $x = 0.15$–$0.20$ have been regarded as promising oxide electrolytes for IT-SOFC as well as electrochemical sensors for monitoring exhaust gases, due to higher values of ionic conductivity than (8YSZ) in the temperature range from 600 to 700 °C. Simple and robust sensing devices that detect carbon monoxide, nitric oxides, sulphur dioxide, and hydrocarbons are needed to meet ever more stringent international combustion reduction goals.[5–7] The main drawback of ceria-based electrolytes, complicating their commercial application is the increase in electronic conductivity under low oxygen partial pressure (below $10^{-10}$ atm) at 800 °C that is accompanied by a reduction of $Ce^{4+}$ to $Ce^{3+}$.[8,9] It has been reported that a reduction of ceria can be neglected at lower temperature around 600–700 °C. However, such low temperatures are not suitable for singly doped ceria as an electrolyte in a SOFC or other devices, due to high electrical resistance.[10]

Structural modification of ceria-based solid solutions by co-doping is one possible way to improve their electrical conductivity at this temperature range. Some ternary system involving $CeO_2$–$Gd_2O_3$ or $CeO_2$–$Sm_2O_3$ have been studied from the viewpoint of structure and electrical conductivity the third components being $Pr_2O_3$,[11] $Y_2O_3$,[12] $Tb_2O_3$,[13] MgO,[14] CaO.[15] Materials co-stabilized with $Gd_2O_3$ or $Sm_2O_3$ and other trivalent cations depending on chemical composition have generally

* Tel.: +48 12 617 25 37; fax: +48 12 617 24 93.
*E-mail address:* potoczek@uci.agh.edu.pl.

0955-2219/$ – see front matter © 2007 Elsevier Ltd. All rights reserved.
doi:10.1016/j.jeurceramsoc.2007.09.004

improved ionic conductivities, although in some cases, deterioration of the ionic conductivity or increase of electronic conductivity was observed.[16]

The present work summarizes a study on the preparation of co-doped ceria solid solutions in the $CeO_2$–$Sm_2O_3$–$Y_2O_3$ or $CeO_2$–$Sm_2O_3$–CaO system and an investigation into those properties crucial to their application as solid electrolytes in IT-SOFC or OBD sensors for monitoring exhaust gases in diesel engine applications.

## 2. Experiments

The pure $CeO_2$, singly or co-doped ceria-based powders in the $CeO_2$–$Sm_2O_3$–$Y_2O_3$ or $CeO_2$–$Sm_2O_3$–CaO were obtained by the citrate method. The starting materials were $Ce(NO_3)_3{\cdot}6H_2O$, $Sm(NO_3)_3{\cdot}6H_2O$, $Y(NO_3)_3{\cdot}6H_2O$, $Ca(NO_3){\cdot}4H_2O$, citric acid (all 99.99% purity, supplied from Aldrich). The reagents were mixed in distilled water in order to prepare pure $CeO_2$, samaria-doped ceria $Ce_{1-x}Sm_xO_2$, co-doped ceria with samaria and calcia $Ce_{1-x}(Ca_{0.5}Sm_{0.5})_xO_2$, wherein $x = 0.15$, 0.20, 0.25, 0.3 or co-doped ceria with samaria and yttria $Ce_{0.8}Sm_{0.2-x}Y_xO_2$, where $x = 0.02$, 0.04, 0.06, 0.08, 0.1, 0.12, 0.16, 0.2. The monohydrate citric acid was added into cerium, samarium, yttrium (or calcium) nitrate solutions. These solutions were evaporated at 70 °C for 24 h to obtain hard gels. The precursors were calcined at 800 °C for 1 h. The powders obtained were rotary-vibratory grounded with the zirconia grinding media for 10 h in anhydrous ethyl alcohol.

The phase composition of all powders and obtained samples were identified by X-ray diffraction method. The crystalline sizes of the starting powders $d_{(XRD)}$ was assessed from X-ray line broadening. A (1 1 1) peak was used to calculate the crystalline size. The specific surface area was measured by one-point BET technique. The samples were outgased at 150 °C in vacuum. The results were used to calculate an equivalent particle size, $d_{(BET)}$. Transmission electron microscopy was used to observe the morphology of obtained powders. The all $CeO_2$-based powders were isostatiscally cold-pressed under 250 MPa. The pellets were sintered at temperature range of 1250–1500 °C. Scanning electron microscopy was used to observe the microstructure of the samples sintered. A numerical analysis of SEM microphotographs (Visilog 4 program—Noesis) taken from the polished and thermally etched surfaces, was applied to measure microstructural parameters, quantitatively. Apparent density of the samples was measured by the Archimedes method. The hardness and fracture toughness were determined by Vickers indentation method. The Niihara approach was used to calculate the fracture of toughness $K_{Ic}$.[17] Electrical properties of the samples were investigated by means of impedance spectroscopy method. The impedance was measured in the automated setup assembled on Solatron 1260 frequency analyzer in frequency range $10^{-2}$ to $10^6$ Hz and in the temperature range around 150–700 °C. The surface of the pellets were covered by platinum electrodes deposited from paste (Heraus, Germany) or in some cases by Pt sputtered in cathodic discharge.

To estimate the oxygen ion transference number of the ceria-based samples, the EMF of the oxide galvanic cell (1) in the temperature range 500–750 °C was measured:

$$Pt|O_2(p_1)||\text{ceramic oxide electrolyte}(O^{2-})||O_2(p_2)|Pt \quad (1)$$

The electromotive force (EMF) of the cell (1) was measured as a function of temperature (550–700 °C) and oxygen partial pressure (from $10^{-8}$ to 1 atm). The ionic transference number ($t_{ion}$) in the sample was calculated basing on the electromotive force (EMF) values ($E_m$) measured for the cell (1) and on the EMF values ($E_t$) obtained for the cell (1) with a pure oxygen ion conductor.

To verify the stability of obtained $CeO_2$-based materials under oxidizing and reducing conditions, the $CeO_2$-based samples were isothermally heat-treated at 800 °C for 15, 50 and 100 h in air or (5 vol.% $H_2$ in Ar) at 800 °C for 24 h.

## 3. Results and discussion

X-ray diffraction analysis shows that all doped or co-doped ceria powders and samples obtained in the $Ce_{1-x}(Sm_{0.5}Ca_{0.5})_xO_2$ or $Ce_{0.8}Sm_{0.2-x}Y_xO_2$ (Fig. 1a) system were monophase materials. Also no other phase than cubic $CeO_2$ (Fig. 1b) was also found in the X-ray diffraction patterns of the samples exposed into (5 vol.% $H_2$–Ar) gas

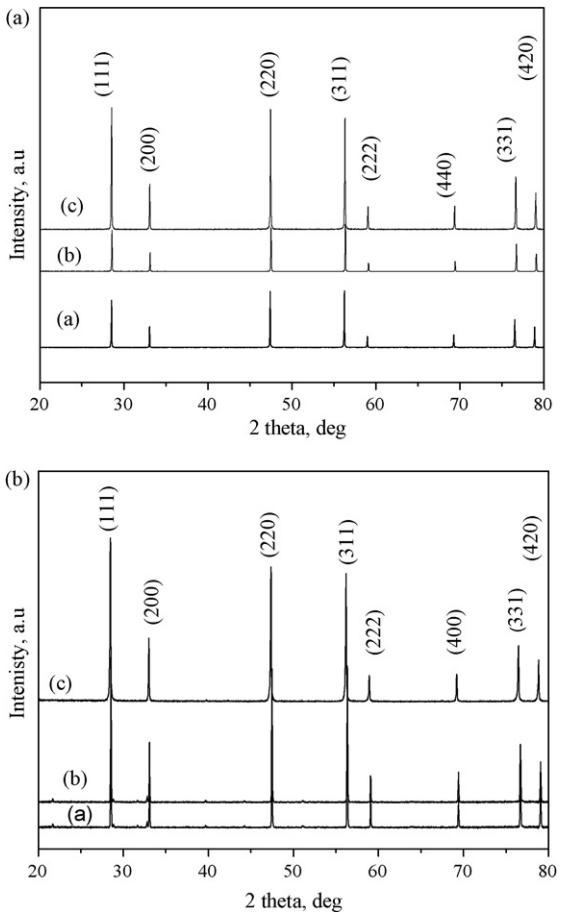


Fig. 1. a XRD diffraction pattern of (a) $Ce_{0.8}(Ca_{0.5}Sm_{0.1})_{0.2}O_2$, (b) pure $CeO_2$, (c) $Ce_{0.8}Sm_{0.06}Y_{0.14}O_2$ samples sintered at 1500 °C for 2 h. (b) XRD diffraction pattern of (a) $Ce_{0.8}Sm_{0.2}O_2$, (b) $Ce_{0.8}Sm_{0.15}Y_{0.05}O_2$, samples after the heat-treatment in 10%$H_2$/Ar at 800 °C for 24 h or $Ce_{0.85}Sm_{0.15}O_2$ (c) in air for 100 h.

Table 1
Basic characterization of selected $CeO_2$-based powders obtained by citrate method

| Composition | $d_{(hkl)}$ | $d_{(BET)}$ |
|---|---|---|
| $CeO_2$ | 17.6 | 22.8 |
| $Ce_{0.8}Sm_{0.2}O_2$ | 24.2 | 28.4 |
| $Ce_{0.8}Y_{0.2}O_2$ | 20.5 | 23.6 |
| $Ce_{0.8}Ca_{0.1}Sm_{0.1}O_2$ | 21.6 | 28.4 |
| $Ce_{0.8}Sm_{0.1}Y_{0.1}O_2$ | 23.3 | 32.8 |

mixture or additionally heated at 800 °C for 150 h in air. Basic characteristic of selected $CeO_2$-based powders are shown in Table 1. The data in Table 1 shows that the crystallite sizes ranged from ~17 to about ~32 nm. The values of equivalent particle size, $d_{(BET)}$, lay very close to those crystallite size, $d_{(XRD)}$. This indicates not extensive contacts between primary particles of the $CeO_2$-based powders and is promising for existence of rather weak agglomerates. The typical TEM microphotography of a $Ce_{0.8}Sm_{0.1}Y_{0.1}O_2$ powder is presented in Fig. 2. The powder consists of isometric particles with a rather narrow particle sizes distribution ranging from 6 to 21 nm. Among them a few agglomerates of about 30–40 nm were also found. All other synthesized powders showed a similar morphology and particle size distribution.

Generally all $CeO_2$-based samples obtained from powders prepared by the citrate method sintered at 1500 °C for 2 h achieved more than 97% of theoretical density. In sample $Ce_{0.7}(Sm_{0.5}Ca_{0.5})_{0.3}O_2$ the decrease of relative density to 93% was observed. Fig. 3a and b shows microstructures of pure $CeO_2$ and $Ce_{0.8}Sm_{0.2}O_2$ samples. Processing of microstructural analysis allowed to determine the grain sizes distributions. Fig. 4 visualizes the variations of average grain sizes of $Ce_{1-x}Sm_xO_2$, or $Ce_{1-x}(Ca_{0.5}Sm_{0.5})_xO_2$ solid solutions versus chemical composition. Contrary to $Y_2O_3$ introduction CaO into solid solution $Ce_{1-x}(Sm_{0.5}Ca_{0.5})_xO_2$ led to increase of grain sizes compared to $Ce_{0.8}Sm_{0.2}O_2$ sample. Samples heated in a hydrogen containing atmosphere were also investigated by SEM. No cracks and additional pores were detected for ceria-based solid solutions in contrast to pure $CeO_2$. Since only gas-tight ceramic elements could be applied as solid electrolytes in electrochemical devices operating in oxidizing and reducing conditions. Compounds in the $CeO_2$–$Sm_2O_3$–$Y_2O_3$ or $CeO_2$–$Sm_2O_3$–CaO system exhibited a high potential. The corrosion resistance of these materials

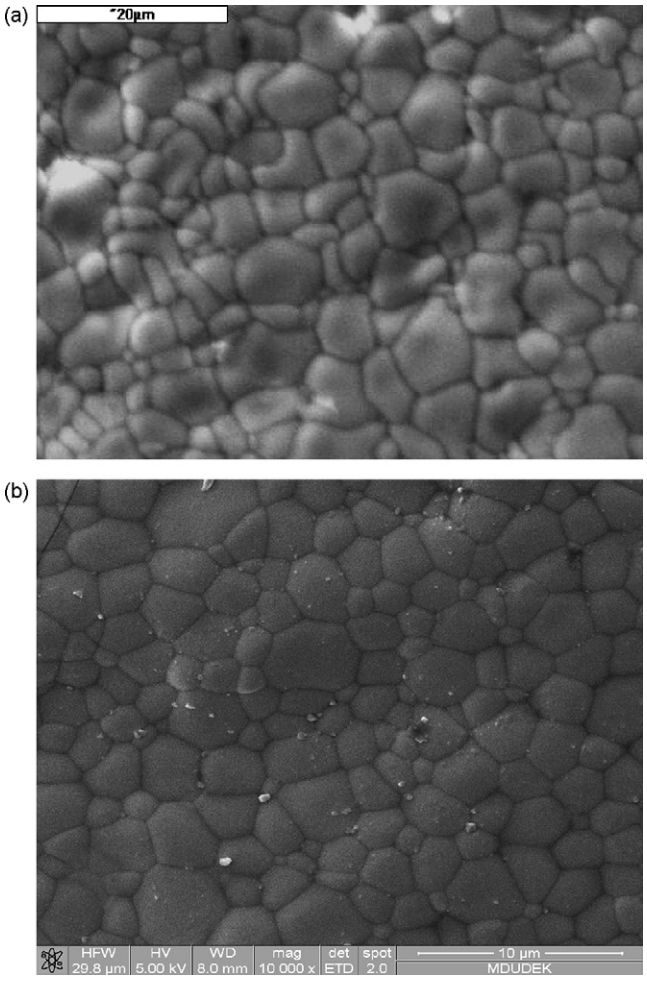


Fig. 3. (a) Microstructure of pure $CeO_2$ (1500 °C, 2 h). (b) Microstructure of pure $Ce_{0.8}Sm_{0.2}O_2$ (1500 °C, 2 h).

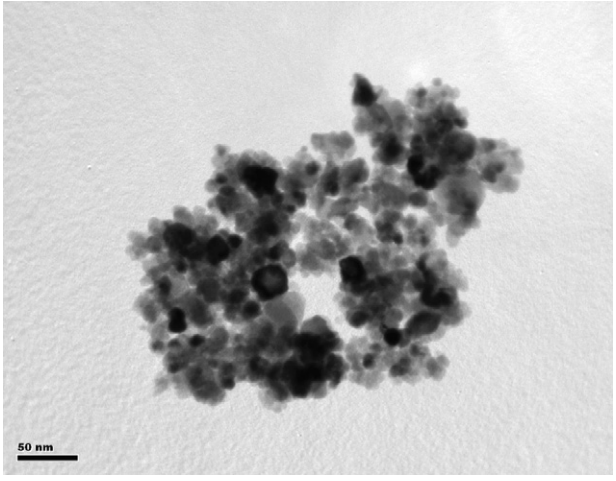


Fig. 2. TEM morphology of $Ce_{0.8}$ $Y_{0.1}Sm_{0.1}O_2$ powder.

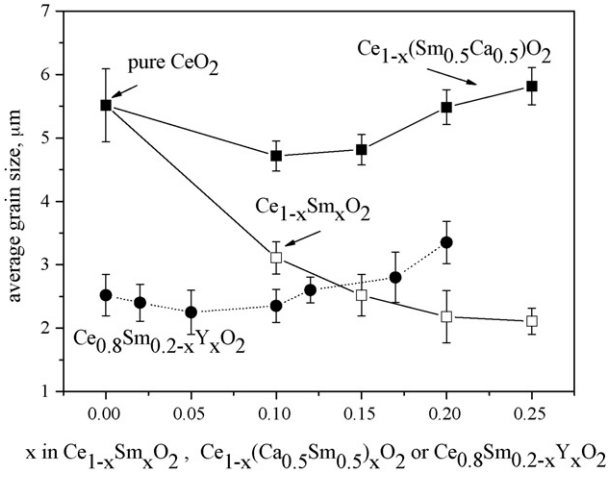


Fig. 4. Changes of ceria average grain sizes vs. chemical composition.

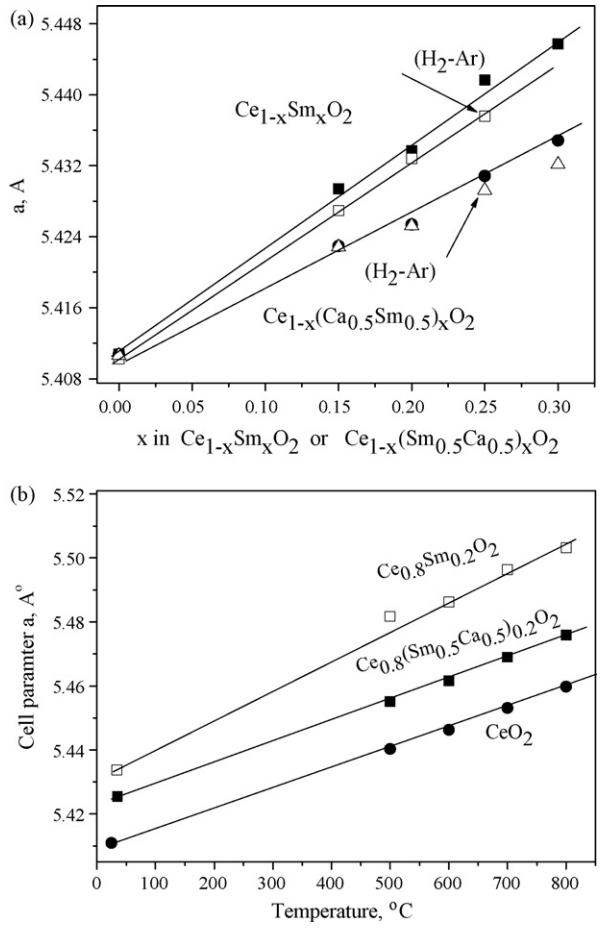


Fig. 5. (a) Dependence of lattice constant on the composition $x$ of $Ce_{1-x}Sm_xO_2$ or $Ce_{1-x}(Sm_{0.5}Ca_{0.5})_xO_2$-based samples. (b) The XRD measurements temperature dependence of cell parameter of selected $CeO_2$-based materials.

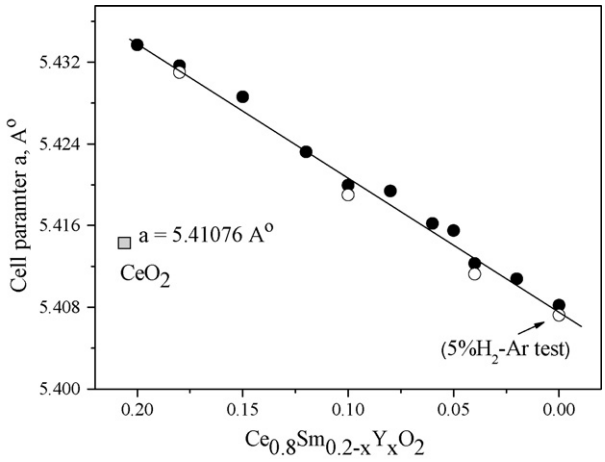


Fig. 6. The compositional dependence of lattice constant of $Ce_{0.8}Sm_{0.2-x}Y_xO_2$ solid solution.

was also tested in the combustion gases from a self-ignition engine. It was found that $Ce_{0.8}Sm_{0.2}O_2$ or $Ce_{0.8}Sm_{0.1}Y_{0.1}O_2$ solid solutions exhibits better corrosion resistance than pure $CeO_2$, or partially $Y_2O_3$-stabilized $ZrO_2$ (3YSZ) in exhaust gases containing sulphur oxide.[18]

The lattice parameter of $Ce_{1-x}Sm_xO_2$ and $Ce_{1-x}(Sm_{0.5}Ca_{0.5})_xO_2$ (Fig. 5a) increase linearly with an increasing $x$ in $Ce_{1-x}Sm_xO_2$, but the slope is lower for the double-doped ceria with $Ca^{2+}$ and $Sm^{3+}$ compared to single-doped ceria. The XRD high temperature measurements (Fig. 5b) performed for selected ceria-based electrolytes indicated that the lattice cell also increased linearly with temperature for the $CeO_2$-based samples. A replacement of $Sm_2O_3$ by $Y_2O_3$ in the solid solution $Ce_{0.8}Sm_{0.2-x}Y_xO_2$ caused the linear decrease of the cell parameter towards lower values close to values of $Ce_{0.8}Y_{0.2}O_2$ as expected from effective ionic radii considerations (Fig. 6), the radius $Y^{3+}$ (0.1159 nm) is smaller than the radius $Sm^{3+}$ (0.1209 nm).[19] An additional heat-treatment in air or (Ar–$H_2$) gas mixtures also caused a small decrease of cell parameters.

The mechanical properties are also important for ceria-based materials as solid oxide electrolytes, which could be used in solid oxide fuel cells and gas sensors working for diesel engine. The determined values of hardness HV and fracture toughness $K_{Ic}$ of the investigated materials are listed in Table 2. This table also compares values of hardness HV, fracture toughness $K_{Ic}$ determined for other ceramic oxide electrolytes from CaO–$ZrO_2$ or $Y_2O_3$–$ZrO_2$ systems, which are considered also as components, which could be applied in IT-SOFC or OBD sensors for monitoring combustion gases in diesel engine.[18] The determined values of hardness HV or fracture toughness $K_{Ic}$ indicates that the all investigated ceria-based materials exhibited slightly lower values for hardness and toughness compared to 8YSZ or 15CSZ. The crack propagation observations for ceria-based samples and 8YSZ electrolyte indicated that cracks propagated both along the grain boundaries and across ceria grains in all investigated materials.

The impedance diagram recorded for $Ce_{0.8}Sm_{0.1}Y_{0.1}O_2$ at 300 °C is shown in Fig. 7. The impedance spectra were fit by equivalent circuits consisting on the series of three sub-circuits of parallel resistor-CPA elements. In some cases even four such sub-circuits were needed in order to obtain low square of fitting. The sub-circuits were attributed to bulk dispersion, one- or two-grain boundary dispersions and electrode dispersion. After successful fitting values of bulk or grain boundary resistors were recalculated to bulk or grain boundary conductivity.

The temperature dependence of the bulk and grain boundary conductivity for the sample $Ce_{0.8}Sm_{0.15}Y_{0.05}O_2$ is shown in Fig. 8 as a $\log(\sigma T)$ versus $1/T$ plot. A single straight line

Table 2
Hardness HV and fracture toughness $K_{Ic}$ of selected ceramic oxide electrolytes, which are considered as components of IT-SOFC and gas sensor in diesel engine

| Material | HV (GPa) | $K_{Ic}$ (MPa m$^{0.5}$) |
|---|---|---|
| $Ce_{0.8}Y_{0.2}O_2$ | 7.90 ± 0.15 | 2.16 ± 0.21 |
| $Ce_{0.8}Sm_{0.2}O_2$ | 8.20 ± 0.20 | 2.30 ± 0.14 |
| $Ce_{0.8}Sm_{0.1}Ca_{0.1}O_2$ | 8.44 ± 0.18 | 2.46 ± 0.21 |
| $Ce_{0.8}Sm_{0.1}Y_{0.1}O_2$ | 8.34 ± 0.21 | 2.28 ± 0.18 |
| $Ce_{0.8}Sm_{0.15}Y_{0.05}O_2$ | 8.40 ± 0.26 | 2.30 ± 0.25 |
| 8% mol $Y_2O_3$ in $ZrO_2$ (8YSZ) | 12.83 ± 0.16 | 2.71 ± 0.16 |
| 15% mol CaO in $ZrO_2$ (15CSZ) | 11.60 ± 0.18 | 2.70 ± 0.31 |

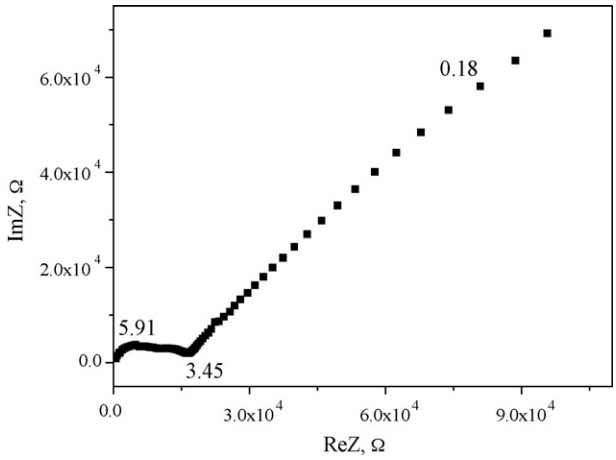


Fig. 7. Typical impedance diagram recorded for $Ce_{0.8}Sm_{0.1}Y_{0.1}O_2$ at 300 °C.

represents the Arrhenius plot of both bulk and grain boundary conductivity. Compositional dependence of bulk and grain boundary conductivity of the system $Sm_2O_3$–$Y_2O_3$–$CeO_2$ at 500 and 700 °C are shown in Fig. 9a and b. The gradually exchange $Sm_2O_3$ by $Y_2O_3$caused the increase of bulk and grain boundary conductivity for small substitution levels until it reaches a maximum at the composition $Ce_{0.8}Sm_{0.1}Y_{0.1}O_2$. The dependence of activation energy of bulk and grain boundary conductivity on composition, shown in Fig. 10, seems to be correlated with compositional variations of conductivity—maximum values of bulk or grain boundary conductivity corresponds to a minimum in activation energy. This behaviour could be related with the lattice distortion away from pure $CeO_2$. The sample $Ce_{0.8}Sm_{0.1}Y_{0.1}O_2$ has a lattice constant more close to pure $CeO_2$ than $Ce_{0.8}Sm_{0.2}O_2$ or $Ce_{0.8}Y_{0.2}O_2$ with the same dopant concentrations. The next reason to explain such dependence could be related to microstructural changes in ceria-based samples. The grain boundary conductivity of $Ce_{0.8}Sm_{0.2-x}Y_xO_2$ increased up to $x = 0.1$ and decreased for high substitution level. The changes of average grain sizes (Fig. 4) shows opposite trend. Fig. 11 also presents the comparison results of total electrical conductivity of $Ce_{0.8}Sm_{0.1}R_{0.1}O_2$

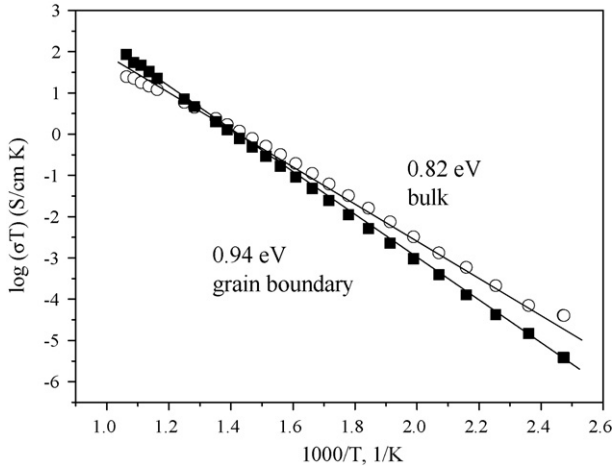


Fig. 8. The temperature dependence of bulk and grain boundary conductivity for $Ce_{0.8}Sm_{0.15}Y_{0.05}O_2$ sample.

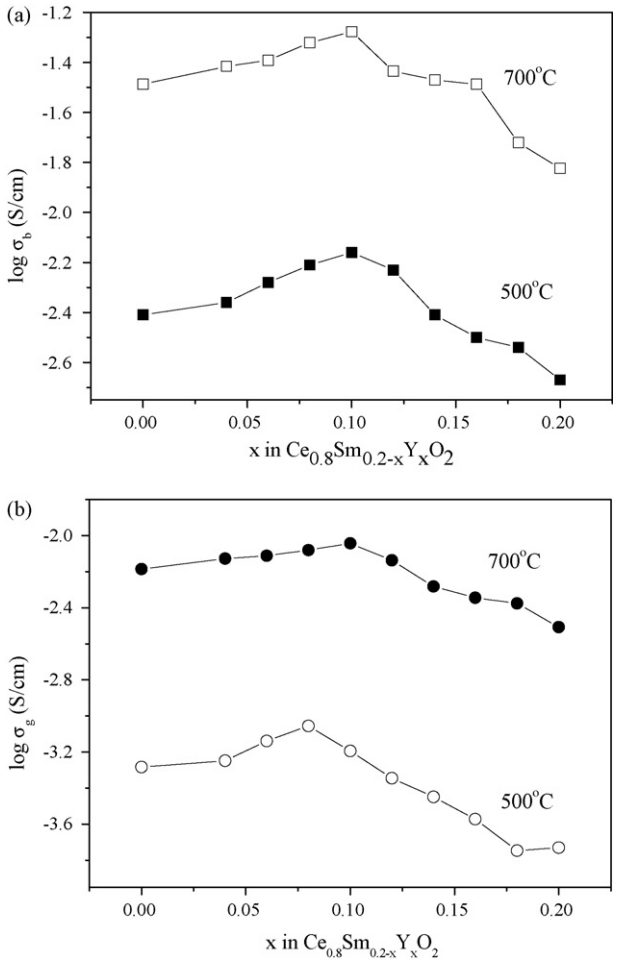


Fig. 9. (a) Bulk conductivity ($\sigma_b$) as function of content $Y_2O_3$ $x$ in $Ce_{0.8}Sm_{0.2-x}Y_xO_2$. (b) Grain boundary conductivity ($\sigma_{gb}$) as function of content $Y_2O_3$ $x$ in $Ce_{0.8}Sm_{0.2-x}Y_xO_2$.

samples, where R = Y, La, Gd. Taking into account relations between chemical composition and structural changes of considered materials, it can state that the highest values of total electrical conductivity correspond to sample with the smallest changes of cell constant compared to pure $CeO_2$.

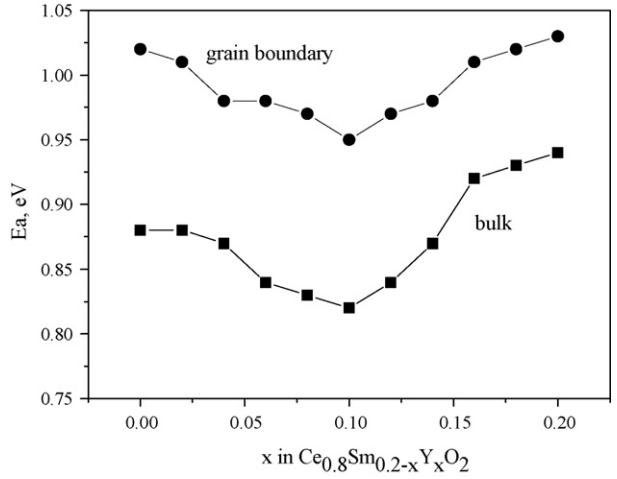


Fig. 10. Activation energy of bulk or grain boundary conductivity as a function of composition.

Table 3
Electrical conductivity at 600 °C of the $CeO_2$–$Sm_2O_3$–CaO or $CeO_2$–$Y_2O_3$–$Sm_2O_3$-based samples

| Composition | $\sigma$ (S/cm), 600 °C | | $E_a$ (eV) | |
|---|---|---|---|---|
| | Bulk | Grain boundary | Bulk | Grain boundary |
| $CeO_2$ | $6.16 \times 10^{-5}$ | $1.21 \times 10^{-6}$ | 1.51 | 1.81 |
| $Ce_{0.85}Sm_{0.15}O_2$ | $3.72 \times 10^{-3}$ | $2.23 \times 10^{-3}$ | 0.89 | 1.02 |
| $Ce_{0.8}Sm_{0.2}O_2$ | $5.21 \times 10^{-3}$ | $4.11 \times 10^{-3}$ | 0.87 | 0.96 |
| $Ce_{0.75}Sm_{0.25}O_2$ | $2.18 \times 10^{-3}$ | $9.85 \times 10^{-4}$ | 0.92 | 0.95 |
| $Ce_{0.7}Sm_{0.3}O_2$ | $4.41 \times 10^{-4}$ | $2.67 \times 10^{-4}$ | 1.01 | 1.12 |
| $Ce_{0.85}(Ca_{0.5}Sm0.5)_{0.15}O_2$ | $3.11 \times 10^{-3}$ | $1.86 \times 10^{-3}$ | 1.11 | 1.16 |
| $Ce_{0.8}$ $(Ca_{0.5}Sm0.5)_{0.2}O_2$ | $7.31 \times 10^{-3}$ | $5.28 \times 10^{-3}$ | 0.80 | 0.90 |
| $Ce_{0.75}(Ca_{0.5}Sm_{0.5})_{0.25}O_2$ | $1.81 \times 10^{-3}$ | $1.08 \times 10^{-3}$ | 0.84 | 0.94 |
| $Ce_{0.7}(Ca_{0.5}Sm_{0.5})_{0.3}O_2$ | $5.21 \times 10^{-4}$ | $4.53 \times 10^{-4}$ | 0.95 | 1.02 |
| $Ce_{0.8}Y_{0.2}O_2$ | $4.68 \times 10^{-3}$ | $1.18 \times 10^{-3}$ | 1.04 | 1.06 |
| $Ce_{0.8}Sm_{0.15}Y_{0.05}O_2$ | $7.26 \times 10^{-3}$ | $4.18 \times 10^{-3}$ | 0.84 | 0.96 |
| $Ce_{0.8}Sm_{0.1}Y_{0.1}O_2$ | $8.16 \times 10^{-3}$ | $7.62 \times 10^{-3}$ | 0.83 | 0.92 |
| $Ce_{0.85}Y_{0.15}Sm_{0.05}O_2$ | $6.15 \times 10^{-3}$ | $4.86 \times 10^{-3}$ | 0.93 | 0.97 |

An improvement of bulk and grain boundary conductivity in $Ce_{1-x}(Sm_{0.5}Ca_{0.5})_xO_2$, with $x = 0.15$, 0.2 or 0.25 sintered samples could also be observed. Conductivities at temperature range from 200 to 700°C, and data for other electrolytes are also given. As shown in Table 3, the bulk and grain boundary conductivity of $Ce_{1-x}Sm_xO_2$ and $Ce_{1-x}(Sm_{0.5}Ca_{0.5})_xO_2$ increased up to $x = 0.20$ and decreased for higher substitution level. The activation energy shows the opposite trend. As previously reported[20] the ionic conductivities are significantly enhanced in $Ce_{1-x}Sm_xO_2$ solid solution by increasing the oxygen vacancies ($V_O^{\bullet\bullet}$) is ascribed to defect association of the type $\{Sm'_{Ce}V_o^{\bullet\bullet}\}$ at higher concentrations of $x$. The introduction of calcia into ceria–samaria solid solutions caused the small increase of values of ionic conductivity. It also could be attributed with reduction of the lattice deviation of the doped ceria from pure $CeO_2$.

The $Ce_{0.8}Sm_{0.1}Y_{0.1}O_2$ and $Ce_{0.8}(Ca_{0.5}Sm_{0.5})_{0.2}O_2$ exhibited the highest values of total electrical conductivity from the $CeO_2$–$Sm_2O_3$–$Y_2O_3$ or $CeO_2$–$Sm_2O_3$–CaO system.

The $Ce_{0.8}Sm_{0.1}Y_{0.1}O_2$ or $Ce_{0.8}Sm_{0.1}Ca_{0.1}O_2$ samples were also tested as solid oxide electrolytes in oxide concentration (1) cells. The linear EMF temperature dependence for

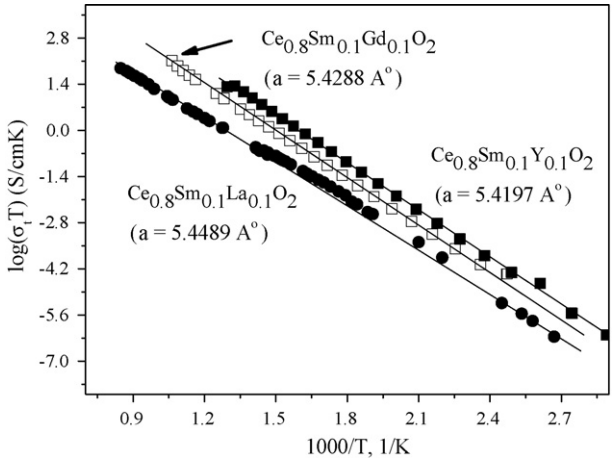


Fig. 11. The temperature dependence of total electrical conductivity of $Ce_{0.8}Sm_{0.1}R_{0.1}O_2$, R = La, Gd, Y samples.

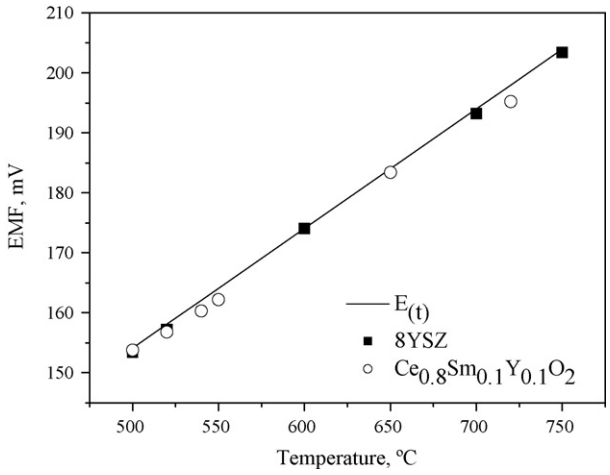


Fig. 12. The EMF of cell (1) temperature dependence. Pt/air was applied as reference electrode, $p_2 = 2 \times 10^{-5}$ (atm).

$Ce_{0.8}Sm_{0.1}Y_{0.1}O_2$ solid oxide electrolyte is shown in Fig. 12. The EMF values of the cell (1) measured in the temperature range of 550–750 °C are compared with the respective EMF ($E_t$) measured with the cell (1) containing 8YSZ. The calculated values of the transference oxygen number $t_{ion}$ of co-doped ceria-based materials are close 1, which indicates practically pure oxygen ion conductivity in the investigated samples at temperatures 550–750 °C and oxygen partial pressure ranging from 1 to $10^{-8}$ atm. The comparison of changes of electrical conductivity versus temperature and oxygen transference number for singly or co-doped $Ce_{0.8}Sm_{0.1}Y_{0.1}O_2$ or $Ce_{0.8}(Sm_{0.5}Ca_{0.5})_{0.2}O_2$ samples indicate that reason of the conductivity enhancement with respect to only samaria-doped ceria is an increase of oxygen vacancy concentrations.

## 4. Conclusions

The dense, gas-tight ceramic samples from systems $CeO_2$–$Sm_2O_3$–$Y_2O_3$ or $CeO_2$–$Sm_2O_3$–CaO were obtained from starting powders synthesized by citrate method. The results presented in this paper indicate that $Ce_{0.8}Sm_{0.1}Y_{0.1}O_2$or $Ce_{0.8}(Ca_{0.5}Sm_{0.5})_{0.2}O_2$ samples seem to be more suitable solid

electrolytes than $Ce_{0.8}Sm_{0.2}O_2$ for application in intermediate solid oxide fuel cells and other electrochemical devices operating in an intermediate temperature range (600–700 °C).

## Acknowledgment

This work was carried out under contract no. 3T08D01926 with the Polish Scientific Research Committee.

## References

1. Subbaro, E. S., Zirconia—an overview. In *Advances in Ceramics*, *vol. 3*, ed. A. H. Heuer and L. W. Hobbs. The American Ceramic Society, Columbus, OH, 1981.
2. Knauth, P. and Tuller, H., Solid state ionics: roots, status, and future prospects. *J. Am. Ceram. Soc.*, 2002, **85**, 1654–1680.
3. Minh, N. Q., Ceramic fuel cell. *J. Am. Ceram. Soc.*, 1993, **73**, 563–588.
4. Badwal, S. P. S., Stability of solid oxide fuel cell component. *Solid State Ionics*, 2001, **143**, 39–46.
5. Inaba, H. and Tagawa, H., Ceria-based solid electrolytes. *Solid State Ionics*, 1996, **83**, 1–16.
6. Mukundan, R., Brosha, E., Brown, D. and Garzon, F., Ceria-electrolyte based mixed potential sensors. *Electrochem. Solid State Lett.*, 1999, **2**(8), 412–414.
7. Izu, N., Shin, W., Matsubara, I. and Maruyama, N., Small-temperature dependent resistive gas sensors using $Ce_{0.9}Y_{0.1}O_2$ as a new compensating material. *Sens. Actuator B*, 2004, **101**, 384–386.
8. Abrantes, J. C. C., Perez-Coll, D., Nunez, P. and Frade, J. R., Electronic transport in $Ce_{0.8}Sm_{0.2}O_{1.9-\delta}$ ceramics under reducing conditions. *Electrochim. Acta*, 2003, **48**, 2761–2766.
9. Xiong, Y., Yamaji, K., Horita, T., Sakai, N. and Yokokawa, H., Electronic conduction of 20% mol $YO_{1.5}$ doped $CeO_2$. *J. Electrochem. Soc.*, 2002, **149**(1), E450–E454.
10. Jung, B. and Huang, T. J., Sintering temperature, microstructure and resistivity of polycrystalline $Ce_{0.8}Sm_{0.2}0_{1.9}$. *J. Mater. Sci.*, 2003, **38**, 2461–2468.
11. Lübke, S. and Wiemhöfer, H., Electronic conductivity of Gd-doped ceria with additional Pr-doping. *Solid State Ionics*, 1999, **117**, 229–243.
12. Maffei, N. and Kuriakose, A. K., Solid oxide fuel cells of ceria-doped gadolinium with praseodymium. *Solid State Ionics*, 1998, **107**, 67–71.
13. Huang, W., Shuk, P. and Greenblatt, M., Hydrothermal synthesis and properties of terbium and praseodymium-doped $Ce_{1-x}Sm_xO_2$ solid solutions. *Solid State Ionics*, 1998, **113–115**, 305–310.
14. Wang, F., Chen, S. and Chen, S., $Gd^{3+}$ and $Sm^{3+}$ co-doped ceria-based electrolytes for intermediate temperature solid oxide fuel cells. *Electrochem. Commun.*, 2004, **6**, 743–746.
15. Wang, X., Lin, Y., Holt, C. and Schwartz, S., Electric conductivity and oxygen permeability of modified cerium oxides. *J. Mater. Sci.*, 2003, **38**, 1073–1079.
16. Mori, T., Dreenan, J., Lee, J., Li, J. and Ikegami, T., Oxide ionic conductivity and microstructures of Sm and La-doped $CeO_2$-based systems. *Solid State Ionics*, 2002, **154–155**, 461–466.
17. Nihihara, K., A fracture mechanisms analysis of indentation inducted Palmquist crack in ceramics. *J. Mater. Sci. Lett.*, 1983, **2**, 221–223.
18. Fuć, P., Merkisz, J., Dudek, M., Małecka, B. and Obłąkowska, D., Application of selected ceramic electrolytes as components of sensors working in OBD system. *Pol. Ceram. Bull.*, 2005, **91**(1).
19. Shannon, R. D. and Prewitt, C. T., Effective ionic radii in oxides and fluorides. *Acta Crystalogr.*, 1969, **B.25**, 925.
20. Hung, W., Shuk, P. and Greenblatt, M., Hydrothermal synthesis and properties of terbium or praseodymium-doped $Ce_{1-x}Sm_xO_{2-x/2}$ solid solutions. *Solid State Ionics*, 1998, **113–115**, 305–310.